micromachines

MDPI

Article

Femtosecond Laser 3D Dynamic Focusing Technology–Mirror Sandblasting and Polishing Combined Process of Monocrystalline Silicon Microlens Array Research

Peng Liu [1,2,3], Jiaqin Yang [1,2,3], Tianfeng Zhou [1,2,3], Aowei Xing [1,2], Wenhan Yang [1,2] and Yichuan Zhang [1,2,*]

[1] State Key Laboratory of Chips and Systems for Advanced Light Field Display, School of Mechanical Engineering, Beijing Institute of Technology, Beijing 100081, China; lpamt@bit.edu.cn (P.L.)
[2] School of Mechanical Engineering, Beijing Institute of Technology, Beijing 100081, China
[3] Beijing Institute of Technology Chongqing Innovation Center, Chongqing 401120, China
* Correspondence: zyc@bit.edu.cn

Abstract

Monocrystalline silicon is an ideal material for infrared optics microlens arrays, achieving excellent performance, but the processing is extremely difficult and poses a challenge to traditional processing processes. In this paper, a new process flow for processing monocrystalline silicon microlens arrays is proposed, combining femtosecond laser three-dimensional dynamic focusing processing technology with sandblasting and polishing finishing technology. Dynamic focusing technology is used to adjust the focus position in real time to adapt to the complex processing needs of three-dimensional structures, and the influence of different laser processing parameters on the processing size and morphology is studied. The mechanism of processing errors and surface defects is proposed to realize the compensation of three-dimensional processing errors. Through experiments and simulations, a 515 nm green light, 100 KHz repetition frequency, power of about 20 W—maintaining the same scanning speed of 3000 mm/s and isotropic filling scanning interval of 5 μm, with an on delay of 0.23 ms, an off delay of 0.12 ms, a corner delay of 0.13 ms, and a null walk delay of 0.24 ms, and a delamination height of 1 μm—were finally selected for the laser processing. The process parameters are feasible and the processing effect is good, providing a new solution for processing hard and brittle materials.

Keywords: femtosecond laser; monocrystalline silicon; microlens arrays; mirror sandblasting and polishing

Academic Editor: Yuankun Lin

Received: 3 July 2026
Revised: 23 October 2026
Accepted: 26 October 2026
Published: 31 October 2026

Copyright: © 2026 by the authors. Licensee MDPI, Basel, Switzerland. This article is an open access article distributed under the terms and conditions of the Creative Commons Attribution (CC BY) license.

1. Introduction

Microlens arrays show great potential and practical value in optical imaging, optical sensing, fiber optic coupling and optical illumination [1–2]. Monocrystalline silicon material has good thermal conductivity, high mechanical strength, high compression and abrasion resistance, high temperature and corrosion resistance, possesses a high refractive index and infrared transmittance [3–4], and is an ideal material for infrared optics microlens arrays. Monocrystalline silicon microlens arrays have been widely used in the fields of infrared optics, microelectromechanical systems and integrated circuits [5–6].

Monocrystalline silicon, an ideal infrared optics microlens array material with excellent performance, is a hard and brittle material with high stability and difficult processing

[7]. This poses a challenge to the processing process, and common microlens array processing methods mainly include precision machining [8], high-energy beam current processing [9], and photolithography processing technology [10]. These processing methods have their own advantages and disadvantages, but the difficulty lies in the high hardness of the material, which is easy to crack, and other properties of the processing process are subject to huge restrictions, or limited by the cost of equipment, processing speed and complexity and other factors; the lack of economy is yet to be overcome through the further optimization of the technology and the industrialization of the promotion. In the face of the single-crystal silicon microlens array processing dilemma, there is an urgent need to seek a new processing solution.

Femtosecond laser processing technology has high-intensity, high-frequency characteristics; very high pulse power density can easily deal with all kinds of difficult-to-process materials, especially those such as monocrystalline silicon or ultra-hard materials [11–12]. In the femtosecond laser processing process and processing objects without contact, the thermal damage area is small to avoid surface deformation and scratches due to contact friction and other adverse consequences, so that in the field of hard and brittle materials, microstructure refinement processing shows great advantages and broad application prospects [13]. Currently, the research on femtosecond laser processing in the field of microlens structure preparation mainly focuses on the processing of concave microlens arrays, and there are relatively few research studies on the processing process of the more difficult convex microlens arrays, and most of the existing research results do not involve the optimization of the post-finishing treatment, which, to a certain extent, restricts the comprehensive enhancement of the performance of the microlens arrays [14].

Based on the above problems, this paper innovatively proposes a set of new process chains, combining femtosecond laser roughing with sandblasting and polishing finishing technology; the principle of the process is shown in Figure 1. Dynamic focusing technology is adopted to adjust the focus position in real time to adapt to the complex processing needs of three-dimensional structures, and the influence laws of different laser processing parameters on the processing size and morphology are studied. The mechanism of processing errors and surface defects is proposed to realize the compensation of three-dimensional processing errors, and experiments of femtosecond laser roughing–mirror sandblasting and polishing finishing of lens unit are carried out to explore the feasibility and effectiveness of the process, and to provide a new solution to the process of processing hard and brittle materials.

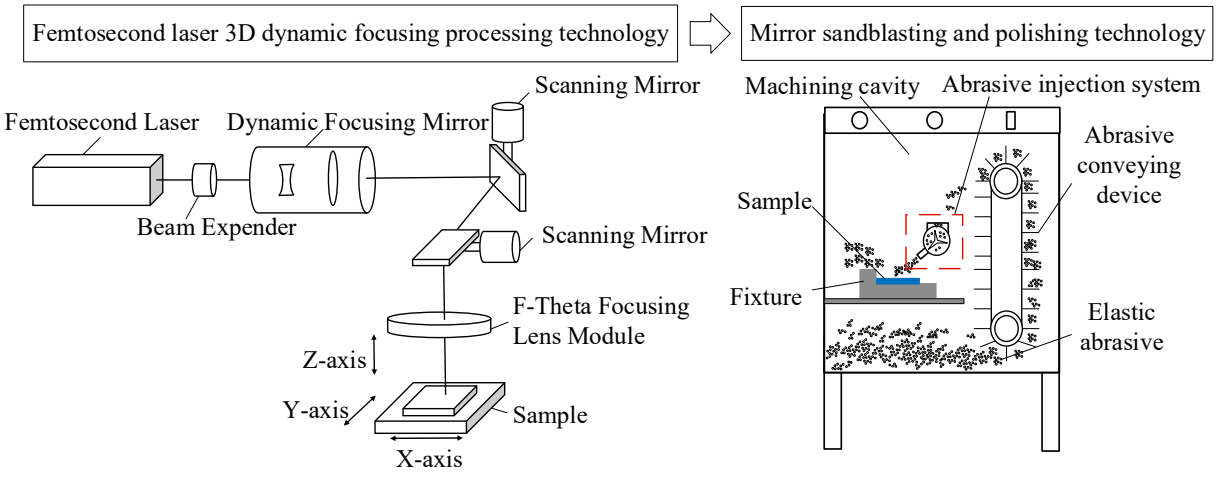


Figure 1. Schematic diagram of femtosecond laser 3D dynamic focusing processing and mirror sandblasting and polishing combined processing technology.

2. Methods

2.1. Processing Mechanism of Femtosecond Laser Three-Dimensional Dynamic Focusing Technology

Ultrafast laser technology has the advantages of high processing precision, low material damage, and a wide range of applications. The high pulse power density of femtosecond laser processing is especially suitable for coping with super-hard materials such as monocrystalline silicon, and the processing process is contactless, with a small area of thermal damage, which avoids undesirable consequences such as surface deformation and scratches due to contact friction [15].

Femtosecond laser processing is achieved by spot sweeping along a specific path, and the formation of the corresponding shape is achieved by a superposition of spots, in which the size of the center distance between two adjacent spots and the coupling distance have a considerable impact on the processing, and the effective number of pulses Q_n can be described by the degree of coupling in the process of femtosecond laser processing, which can be calculated by the following formula (1):

$$Q_n = \frac{2w_0 f}{V} \tag{1}$$

In the above equation, V denotes the scanning speed of the galvanometer; w_0 denotes the radius of the spot girdle; and f denotes the laser repetition frequency.

2.1.1. Femtosecond Laser Single Pulse Processing Monocrystalline Silicon Material Removal Mechanism

The single-pulse ablation mechanism of femtosecond laser is a complex process involving multiple factors [16], and a variety of removal mechanisms occur during processing, mainly phase explosion, thermal melting, non-thermal melting, Coulomb explosion, and opto-mechanical destruction. In the process of femtosecond laser interaction with the workpiece material, elements such as energy density, wavelength, pulse width, repetition frequency, and the properties of the material itself all play a crucial role [17–18].

According to the research of many scholars, femtosecond laser and monocrystalline silicon material role in the process, monocrystalline silicon material needs to be mainly carried out a complex microscopic change process [19].

First of all, the valence band electrons in the valence band of single-crystal silicon, under the femtosecond laser's instantaneous processing of the high peak power, will be in the form of single-photon or multi-photon absorption jump to the conduction band, or absorb more energy; the conduction band in the free electrons will be excited to a higher energy state, the occurrence of collision ionization; and excitation of free electrons in the femtosecond order of magnitude of the time, the scattering of each other to become a true sense of the free electrons. These laser-excited electrons in the instantaneous temperature is extremely high, its temperature far exceeds the lattice, so that the internal thermal equilibrium state is destroyed. This leads to the occurrence of heat transfer between the electrons and the lattice; the free electrons, through the scattering of electrons and electrons and phonon, will continue to transfer energy to the lattice; and a portion of the energy of the free electrons, through a variety of compounding and diffusion mechanisms, and ultimately returned to the valence band or transferred out of the excitation region, the material internal recovery of the original thermal equilibrium. When the laser pulse width is less than 10 ps order of magnitude, the laser pulse damage to the material will be gradually transformed from conventional thermodynamic damage to non-thermodynamic cold damage, macroscopic material near the surface of the region of the explosive phase transition, the solid monocrystalline silicon material is directly transformed into a high-density gasification of high-temperature, high-pressure plasma, which is immediately

repelled by the Coulombic force quickly out of the metal surface, the formation of an effective material removal phenomenon [20–21].

As the plasma sputtering process takes away almost all the energy, the heat-affected zone of femtosecond laser ablation of monocrystalline silicon material is small, and the ablation area has a clear contour [22].

In practical applications, the unique properties of femtosecond lasers can be better utilized to achieve efficient, precise and micro–nano-scale processing of materials through precise tuning of laser parameters and optimization of processing strategies.

2.1.2. Dynamic Focusing Mirror Principle

Femtosecond laser three-dimensional dynamic focusing scanning system breaks through the traditional two-dimensional galvanometer scanning system can not meet the complex three-dimensional structure of the object actual processing needs of this bottleneck, in the field of precision machining, testing and other areas to show the significant value of the application.

The three-dimensional dynamic focusing scanning system is schematically shown in Figure 2, which is combined with a two-dimensional galvanometer scanning system to jointly realize the processing of any position in three-dimensional space. The core element is a pair of positive and negative mirror group combination, the laser beam first through the negative mirror group, by the dispersion effect, and then after the dispersion of the beam and then through the positive mirror group, by the aggregation of the role of the formation of a precise focus. There are two common combinations of mirrors for dynamic focusing systems: non-linear lever structure and linear lever structure, both of which are designed to flexibly change the spacing between the mirrors through their respective mechanical designs, thus precisely regulating the focus position and always keeping the focus on the surface of the 3D machined structure. The system combines the high-speed scanning characteristics of a 2D scanning galvanometer with the real-time focus adjustment capability of a dynamic focusing mirror, and employs telecentric F-Theta field mirrors in order to further optimize beam transmission and focusing effects [23–24].

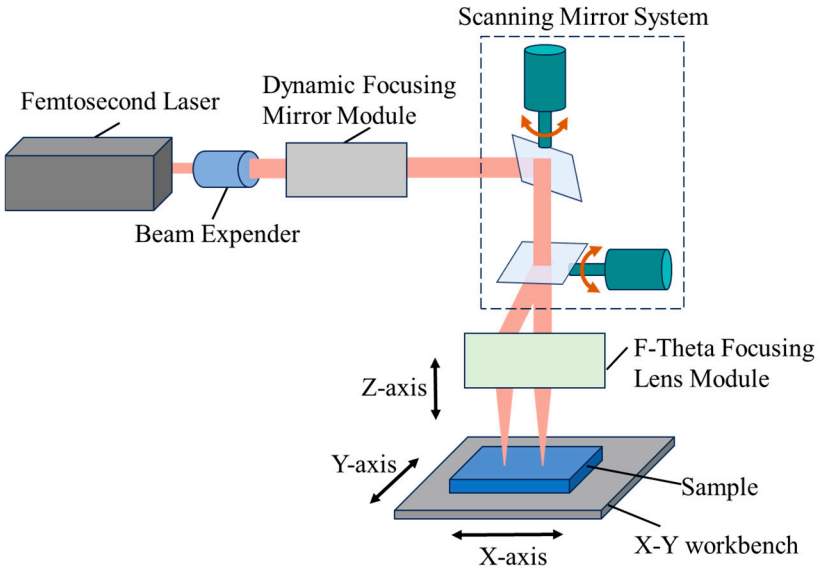


Figure 2. Diagram of 3D dynamic focus scanning system.

Three-dimensional dynamic focusing processing technology through layered dynamic focusing scanning processing: when the height of the workpiece to be processed is within the dynamic focusing mirror focus adjustment range, the height of the workpiece

to be processed can be layered, turning a three-dimensional structure into a number of two-dimensional structures for processing, and two-dimensional structures superimposed on the effect of the structure become a three-dimensional structure. Study the current parameters of laser etching a layer of the material removed by the law; for each layer of material removed, the laser focus moves down a layer through the dynamic focusing mirror to adjust the laser focus, using motors to control the focus to re-focus on the surface of the processed workpiece until this layer of planar scanning is complete, and then the focus is moved again to a layer. Finally, repeat the processing until all the layering is completed, and, ultimately, process the ideal three-dimensional structure.

This experimental equipment is shown in Figure 3. The three-dimensional dynamic processing system part of the femtosecond laser processing equipment consists of a femtosecond laser, beam-expanding mirrors, dynamic focusing mirrors and a vibrating mirror system. The laser light source used for Light Conversion's CARBIDE CB3–80 W (Vilnius, Lithuania) model femtosecond laser—with 0.3–10 ps pulse width harmonic tuning range, 100–2000 kHz base repetition frequency, less than 20 ms full-range power modulation response time and free conversion of the laser wavelength of the automatic harmonic system (1030 nm, 515 nm and 343 nm)—can realize the burst pulse mode with the pulse string interval ranging from picoseconds to nanoseconds; together with the excellishift 3D zoom module with good Z-axis dynamics and the 5-axis carrier stage with the repetition accuracy of ±1 μm, it has the reliability and beam stability adapted to different environmental conditions. It can meet the processing requirements of this experiment.

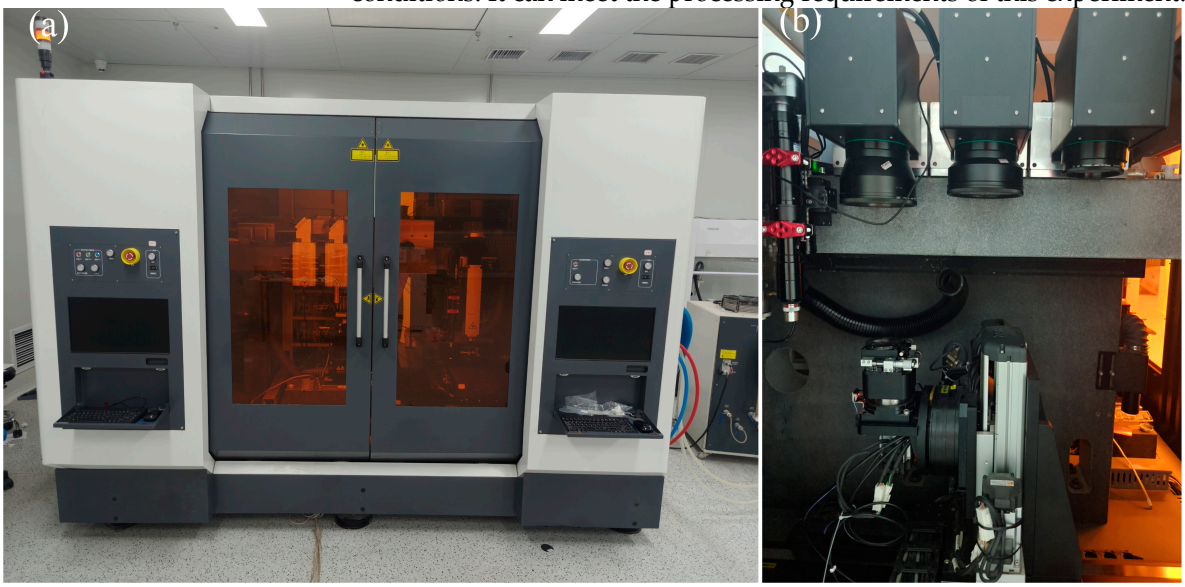


Figure 3. Laser processing equipment: (**a**) Ultrafast Laser Processing Center; (**b**) Laser 3D Dynamic Focusing 5-Axis Machining System.

In this study, mirror sandblasting and polishing were employed as the finishing process following femtosecond laser machining. The process was performed using an SMKS mirror sandblasting machine, as shown in Figure 4, in which abrasive particles were propelled onto the workpiece surface under controlled pressure and angle to achieve material removal and surface polishing.



Figure 4. SMKS mirror surface sandblasting machine.

2.2. Simulation of 3D Dynamic Scanning Machining System in ZEMAX

2.2.1. Initial Setting of Simulation Data

The optical design simulation of the dynamic focusing system uses the ZEMAX (Ansys Zemax OpticStudio 2023 R1.00 Premium) optical simulation software, selects the moving distance of the negative lens to be 10 mm, and the corresponding system lever ratio is set to be 6:1, which not only ensures a sufficient focusing range, but also suppresses to a certain extent the deviation brought about by the lever mechanism, and realizes that the light beam incident to the dynamic focusing part can be effectively moved to focus in a space of 30 mm, so as to achieve the precise processing in three-dimensional space.

Dynamic focusing mirror module, in order to balance the overall size of the system and the ease of installation, set the focal length of the first lens $f_1 = 200$ mm, the focal length of the third lens $f_3 = 600$ mm, and, at the same time, deduced that the focal length of the second lens $f_2 = 349.9$ mm. The positive lens is selected to be the negative lens as the first lens in the system, and the original value of the positive focusing distance is given a negative value, i.e., $f_1 = -200$ mm.

The F-Theta lens module, using the classic four-piece F-Theta objective lens structure as a base model, is used for optimization and simulation. The initial structure consists of four separate lens elements, numbered 1 to 4 in order from left to right, each with a double-sided curvature design and data in millimeters (mm).

Based on the specific conditions of the subsequent processing experiments, the selected telecentric field mirror needs to be matched with a green-light galvanometer system, in which the femtosecond laser wavelength emitted by the galvanometer is 515 nm. The lens material is a high-quality optical material selected from F_SILICA, which possesses a lower dispersion coefficient and higher transmittance, and is effective in reducing chromatic aberration and other aberrations. The diameter of the entry pupil is set to 14 mm, which determines the effective diameter of the beam received by the first stage of the lens entering the system.

2.2.2. Optimization Parameters and Simulation Results

For the dynamic focusing part, there is the basic structure of the zoom module in ZEMAX, and a set of basic structure is selected as the lens of the dynamic focusing part, and the final structure model is obtained by modifying the lens parameters and setting the evaluation function to optimize the structure.

The diameter of the incident pupil is set to 14 mm, F_SILICA glass is chosen as the lens material, the wavelength is selected to be 515 nm, and the Apodization Type is a Gaussian distribution. The overall structure is optimized by setting the evaluation function so that the system achieves the expanding effect of focus shift. For the actual

processing conditions, the lens model used in the simulation is relatively simplified. After a careful parameter optimization process, and combined with the initial structure, the final structural parameters of the system are shown in Figure 5, and its specific key parameters are set in Table 1.

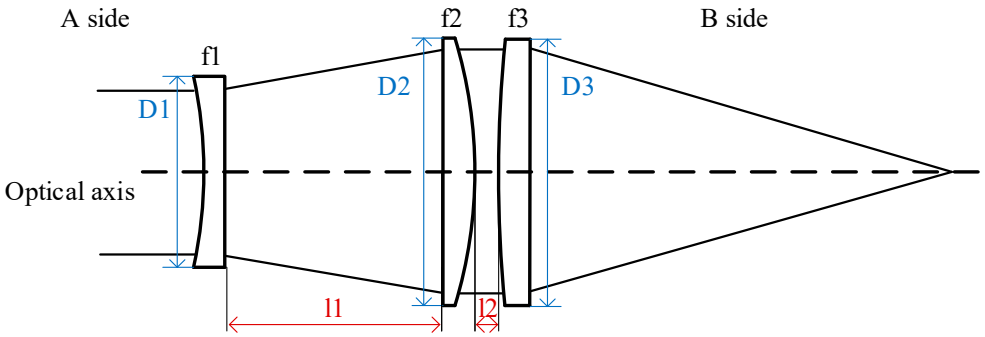


Figure 5. Dynamic focusing mirror structure.

Table 1. Parameters of focusing lenses (unit: mm).

Material: F_SILICA							
	D1	D2	D3	l1	l2	H_{f1}	H_{f2}
Parameters	10	20	20	100	1	3	3
	H_{f3}	f1−ϱ_A	f1−ϱ_B	f2−ϱ_A	f2−ϱ_B	f3−ϱ_A	f3−ϱ_B
Parameters	5	−93.305	/	/	−161.516	276.919	/

H—thickness; ϱ—radius of curvature.

For the F-Theta lens part, an optimization function is constructed to ensure that the focal length of the whole optical system reaches 100 mm. After a series of fine adjustments, the final structural model of the F-Theta lens is shown in Figure 6, and the specific parameters are set as in Table 2.

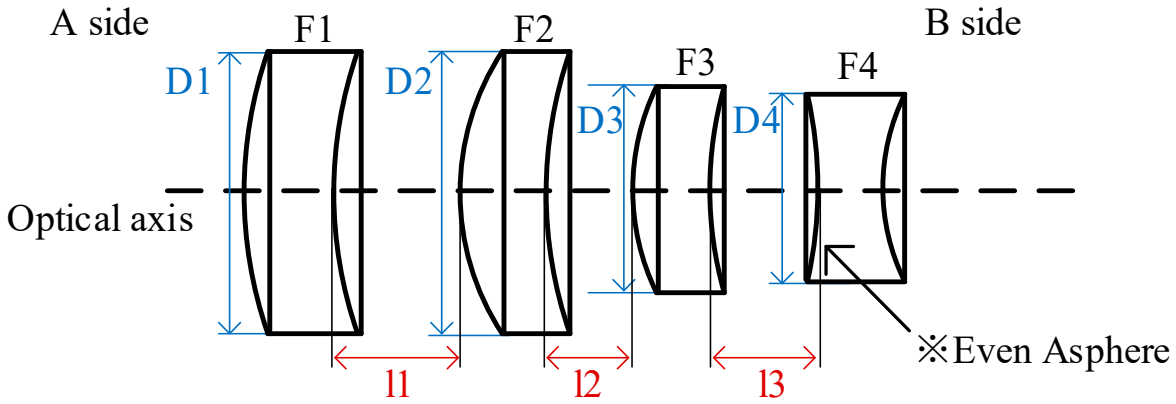


Figure 6. F-Theta lens structure.

Table 2. Parameters of F-Theta lenses (unit: mm).

Material: F_SILICA						
	D1	D2	D3	D4	l1	l2
Parameters	20	20	15	10	12.997	2.989
	l3	H_{f1}	H_{f2}	H_{f3}	H_{f4}	F1−Q_A
Parameters	6	10	11	11	9.799	36.319
	F1−Q_B	F2−Q_A	F2−Q_B	F3−Q_A	F3−Q_B	F4−Q_B
Parameters	24.717	22.010	43.995	22.916	29.411	24.449

Among them, the A side face type of F4 is even aspheric, and the rest of the lens face types are standard. The set face type of an even-order aspheric surface is described by the even powers of radial coordinates to describe the aspheric surface. Its parameters are set as in Table 3, and the equation of face type coordinates is as in (2):

$$z = \frac{cr^2}{1+\sqrt{1-(1+k)c^2r^2}} + a_1r^2 + a_2r^4 + a_3r^6 + a_4r^8 + a_5r^{10} + a_6r^{12} + a_7r^{14} + a_8r^{16} \quad (2)$$

Dynamic focusing part and F-Theta lens part of the two together with the whole with ZEMAX simulation system, the focus of the system can be floating through the dynamic focusing mirror can move the lens distance to observe the rule of change. In the dynamic focusing system and field mirror system connected through the reflector, the dynamic focusing mirror third lens second side and vibration mirror reflector at a distance of 400 mm and the reflector from the first side of the first lens of the F-Theta distance of 100 mm can be obtained from the final simulation of the dynamic focusing and the F-Theta mirror combination system optical path diagram, as shown in Figure 7.

Table 3. Parameters of F4 lens (unit: mm).

F4–A Side	**Parameters**
F4−Q_A	−184.77
F4−k_A	1643.61
F4−a_2	0
F4−a_4	$-6.740935025678001 \times 10^{-5}$
F4−a_6	$1.406176539418000 \times 10^{-7}$
F4−a_8	$-1.286514383215000 \times 10^{-9}$
F4−a_{10}	0
F4−a_{12}	0
F4−a_{16}	0

K—conic curvature.

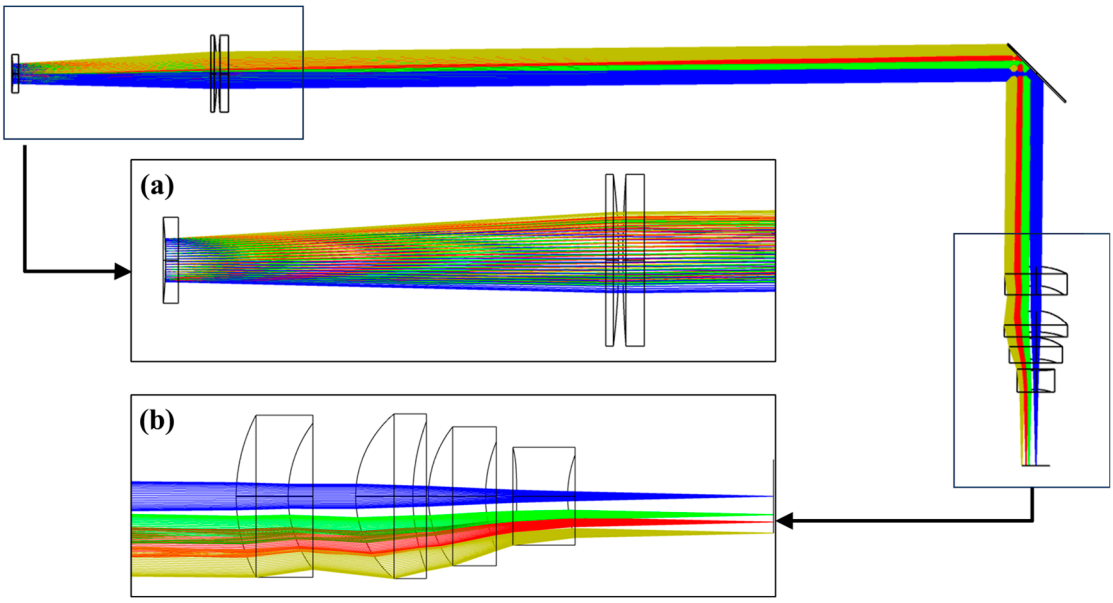


Figure 7. Optical path diagram of 3D dynamic focus scanning system. (**a**) The focusing lenses; (**b**) the F-Theta lenses.

The three-dimensional dynamic focusing system adjusts the focal position along the Z-axis by changing the spacing between the lenses in the dynamic focusing module. During layered machining, the focal position is adjusted according to the machining depth, allowing the laser beam to remain focused on the corresponding processing layer. The ZEMAX simulation illustrates the optical path configuration and demonstrates the feasibility of focal position adjustment. Furthermore, the successful fabrication of monocrystalline silicon microlens arrays using the proposed layered machining strategy provides experimental evidence of the feasibility of the dynamic focusing approach. However, the current simulation mainly focuses on the optical path characteristics, and the variations in spot size and optical aberrations at different Z-axis focusing positions have not been quantitatively evaluated. Therefore, further investigation is required to comprehensively assess the focusing uniformity and optical performance over the entire focusing range.

3. Experiment

3.1. Material

The material chosen for this experiment is monocrystalline silicon wafers with a crystalline surface (110). The dimensions of the experimental wafers are: diameter 5 mm, thickness 3 mm, and surface roughness < 3 nm. The characteristic parameters of monocrystalline silicon material are shown in Table 4.

Table 4. Characteristic parameters of monocrystalline silicon.

P3.	Si
Density（g/cm3）	2.23
Mohs Hardness	7
Young's Modulus E (GPa)	103.9
Shear Modulus G (GPa)	79.9
Refractive Index	3.4

Femtosecond laser three-dimensional dynamic focusing technology is used to process the microlens array on this silicon wafer material. The unit morphology of the target microlens array is a convex hemisphere, and the target experimental parameters are:

radius of 1.95 mm, height of 1.69 mm, unit spacing of 4 mm, and the curvature diameter of 3.9 mm, as shown in Figure 8a. Considering the efficiency and cost, a 2 × 2 array structure is selected for processing, and the inverse model of processing is shown in Figure 8b.

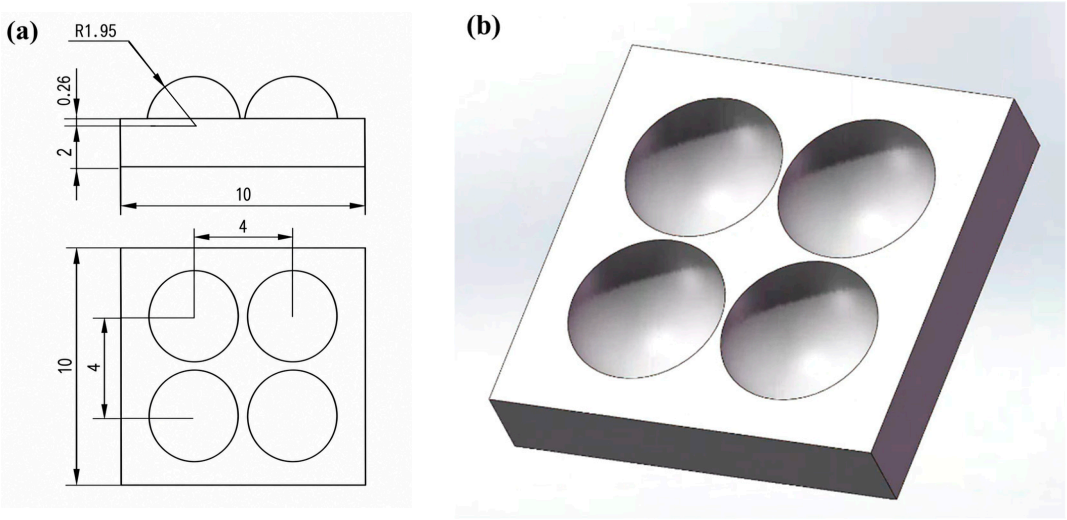


Figure 8. Workpiece target machining drawings and removal models: (**a**) Process drawing; (**b**) removal model.

In order to ensure the accuracy and repeatability of the experiments, all silicon wafers are pre-treated before experimental processing, and ultrasonic cleaners are used to remove possible contaminants and particles on the surface to ensure the surface finish of the material processed, followed by drying using a compressed air gun, and then the processing experiments are carried out.

3.2. Condition

The experimental processing steps are as follows:

(1) Establishment of three-dimensional model: The processing structure of the target microlens array unit is analyzed, the appropriate laser processing method is selected through pre-laboratory work, the processing parameters are determined, and the actual processing model is inquired inversely according to the processing deviation.

(2) Material pretreatment: The surface of the silicon wafer sample to be processed is cleaned by ultrasonic waves, blown dry with pure air after cleaning, and fixed on the platform of the processing system.

(3) Laser three-dimensional layered processing: Select the appropriate laser processing parameters and utilize the dynamic focus mirror to dynamically move the focus for layered processing. Process a 4 × 4 lens array unit and a single lens unit for verification experiments.

(4) Sandblasting and polishing finishing: After processing, ultrasonic cleaning is performed to remove the debris adhering to the processed surface, and the structure is blast-polished for finishing after drying.

After processing, a tactile profiler is used to observe the surface morphology of each cell of the microlens array.

4. Results and Discussion

4.1. Parameter Selection

4.1.1. Selection of Laser Processing Parameters

In this experiment, it is expected that the processed microlens array has very high requirements for surface quality and edge quality, and in order to ensure the clarity of each microlens edge and the overall uniformity, the isotropic filling scanning processing method is selected. For the selection of processing parameters, the fixed parameters of the pre-experiment were pulse width 261 fs, laser wavelength 515 nm, and repetition frequency 100 kHz. Through the control variable method, the evolution law of the laser power and scanning speed on the microstructures processed by the femtosecond laser was studied, and the appropriate parameters were selected.

The laser power is selected as 12 W, 16 W, 20 W and 24 W, and the scanning speed is from 1000 mm/s to 5000 mm/s with a gradient of 500 mm/s. Experiments are carried out to study the etching depth and the law of surface roughness in different cases by machining a 1 mm × 1 mm square slot structure, and the square slot is experimented with by isotropically filling the scanning intervals of 10 μm with the laser etching continuously for 100 times; its evolution law is shown in Figure 9.

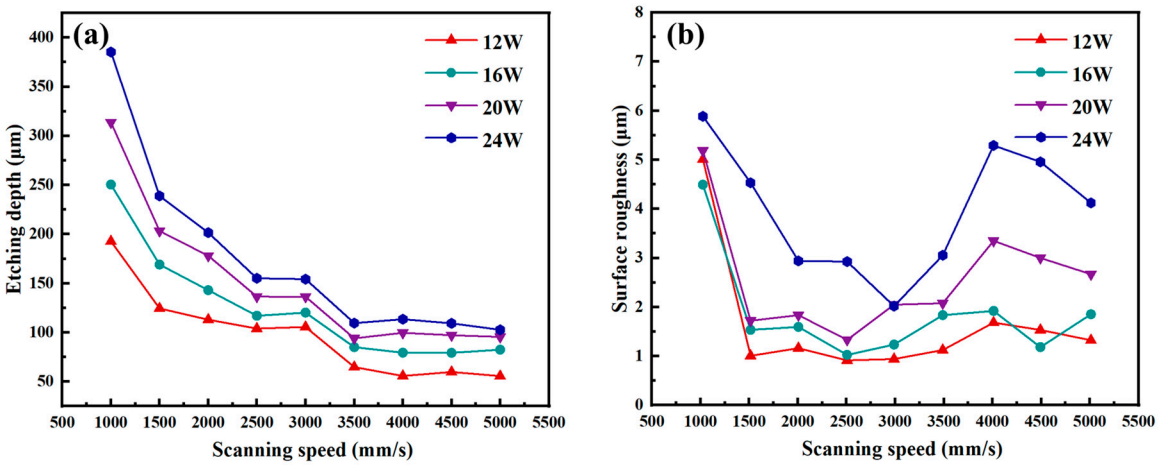


Figure 9. Evolution of etching depth and surface roughness. (**a**) Evolution law of etching depth; (**b**) evolution of surface roughness.

The experimental results show that with the gradual increase in the laser power, the energy density of the focal region increases, and the higher energy density endows the laser with stronger material removal ability, which is an effective way to improve the processing efficiency. With the gradual increase in scanning speed, the effective action time of a single laser pulse on the material surface is shortened, while the number of pulses acting per unit time is reduced; this change directly affects the intensity of the thermal accumulation effect, reducing the continuous heating time and local temperature of the material, making it easier for the material in the ablation process to solidify more quickly. Although the laser energy is concentrated in a short period of time, the amount of material actually removed decreases due to the rapid cooling of the material, and thus the ablation depth is observed to decrease gradually with the increase in scanning speed, as shown in Figure 9a.

As the energy density increases, laser ablation not only deepens the etching depth, but also expands the affected area, resulting in further exposure or even exacerbation of structural defects on the surface of the material and in the near-surface layer, resulting in an increasing trend in surface roughness. This growth is not linear; in a certain energy

density interval, the growth trend is not very obvious, which may be due to material removal and thermal effects to achieve a certain dynamic equilibrium, and once this threshold is exceeded, with the further increase in energy density, the surface roughness will be suddenly intensified, reflecting the material surface due to the overly strong thermal effects suffered by the intense damage, as shown in Figure 9b.

The surface roughness of the groove features is shown in Figure 10. As shown in the figure, in the low-velocity region (<2000 mm/s), the higher thermal accumulation leads to a significant surface quality degradation. Due to the short pulse intervals, the superposition of neighboring pulse energies causes the bottom of the material to repeatedly undergo the melting and solidification process, forming micro-fold structures, as well as typical defects such as craters and recast layers, as shown in Figure 10a. Such times not only increase the surface roughness, but also reduce the overall quality and consistency of the machined area.

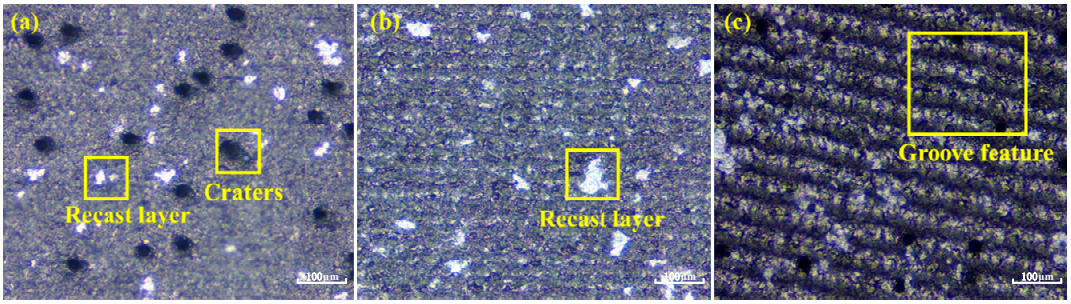


Figure 10. Surface machining topography at different speeds: (**a**) low speed (<2000 mm/s) processing surface topography; (**b**) medium speed (2000 mm/s–3500 mm /s) processing surface topography; (**c**) high speed (3500 mm/s–5000 mm /s) processing surface topography.

In the medium-speed zone (2000 mm/s–3500 mm/s), the thermal accumulation effect is significantly weakened, and the change in surface roughness tends to stabilize, and laser processing reaches an equilibrium point in this speed range. At this time, although the crater morphology basically disappeared, there still existed a small amount of recast material, indicating that although the thermal influence has been significantly reduced, the energy distribution is still insufficient to completely avoid the local overheating phenomenon, as shown in Figure 10b.

In the high-speed region (3500 mm/s–5000 mm/s), the surface roughness increases significantly again. This change stems from the low laser energy received at a single point, resulting in a significant reduction in the effective processing area at the focal point, where the laser only forms an effective etching area in the center of the path, while the surrounding area is not fully processed due to insufficient energy. This uneven removal process eventually resulted in the formation of square grooves with continuous groove features and a significant increase in surface roughness, as shown in Figure 10c.

Femtosecond laser direct ablation by layer-by-layer material removal processes the three-dimensional structure of the continuous surface. Different laser processing parameters for single-layer removal of different amounts, such as the removal of a larger amount, will produce a step-like surface, so the selection of parameters is quite important. Based on the data in this section of the study, taking into account the quality of the surface and the processing efficiency of the problem, the final selection of the laser parameters is as follows in Table 5.

Table 5. Selection of laser parameters.

Parameters	Value
Wavelength	515 nm
Repeat frequency	100 KHz
Power	20 W
Scanning speed	3000 mm/s
Layer height	1 μm
Isotropic filling interval	5 μm

4.1.2. Selection of Laser Delay Parameters

Laser processing starts and terminates at moments when the scanning speed is relatively low because the galvanometer motor has not yet reached or is in the process of decelerating, and the laser pulse coupling rate changes as a result. Higher coupling rates at the beginning and end of the process mean that the laser energy is absorbed more fully during these times, resulting in greater material removal in this area than in the middle of the process. The final processed surface has a "crater" irregular shape with impaired edge quality, which is a significant deviation from the expected ideal microstructure.

In order to ensure the accuracy of femtosecond laser large-area filling processing in femtosecond laser equipment, the laser light source out of the laser is much faster than the response speed of the scanning galvanometer control system, and the laser delay parameter is to set the advance pre-response time of the process parameters. The delay method analyzes the laser delay on the large-area filling processing accuracy of the law, in the design of processing scanning path in advance compensation, as shown in Figure 11. The essence of this method is to wait for the scanning galvanometer system to stabilize its operation before starting or shutting down the laser to eliminate the edge error.

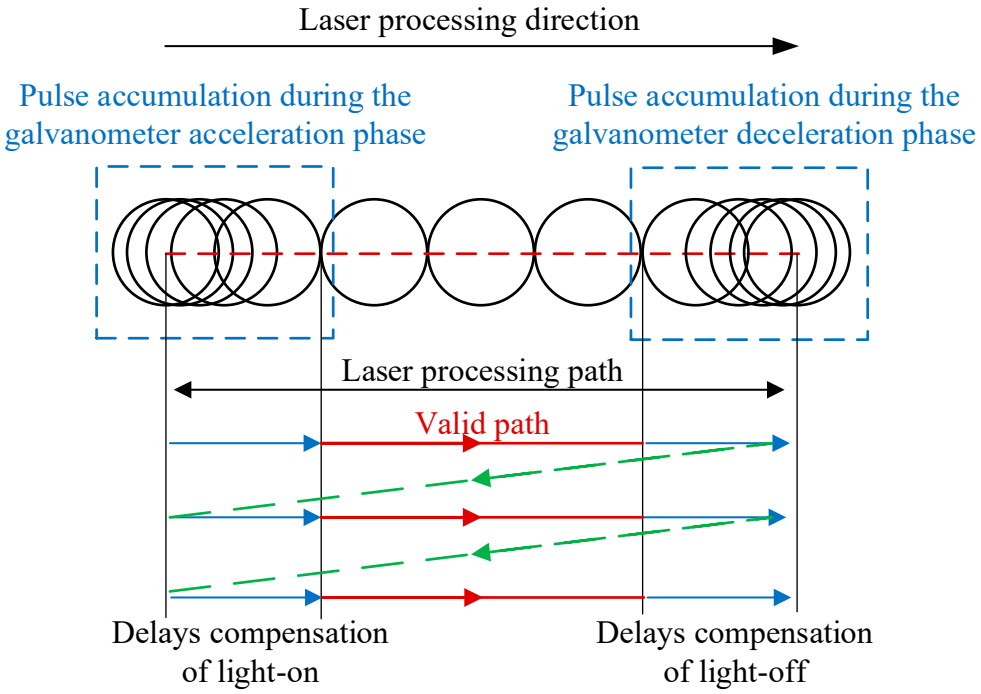


Figure 11. Isotropic scanning delay compensation principle.

Considering the effects of etching depth and surface roughness, the switching delay is mainly related to the scanning speed of the galvanometer, and different scanning speeds require different delay parameters in order to obtain a flat edge surface quality. The switching delay was chosen to be 1000 mm/s for the switching delay experiment. The

switching delay was graded at 0.5 ms, and the range was 0–3 ms for the crossover experiment. Finally, based on the measurement results of the above experiments and the twelve equal circle experiments, each parameter was selected as shown in Table 6. With these parameters, when measuring the edge of the square groove, it can be observed that there is no trace of pulse accumulation on the edge, which has basically eliminated the edge error, ensured the stability of the machining process, and realized the compensation effect.

Table 6. Delay parameter selection.

Parameters	Turn On Delay Time	Turn Off Delay Time	Turn Angle Delay Time	Empty Travel Delay Time
Value	0.23 ms	0.12 ms	0.13 ms	0.24 ms

4.2. Femtosecond Laser 3D Dynamic Focusing Processing and Error Compensation

4.2.1. Feasibility of Process Parameters

The size of the laser focusing spot has a decisive influence on the final processing effect, and a smaller spot size is needed to obtain a good processing shape. According to the focusing formula of a Gaussian beam, the diameter D of the focused spot at the focal point can be shown by Equation (3).

$$D = \frac{4\lambda f M^2}{\pi D_i} \tag{3}$$

where D_i is the laser spot diameter incident on the F-Theta field mirror; f is the effective focal length of the F-Theta field mirror; λ is the laser wavelength; and M^2 is the beam quality factor.

The wavelength of the femtosecond laser selected for this experiment is 515 nm, the effective focal length of the field mirror is 160 mm, the M^2 factor is 1.1, and the spot diameter of the light beam incident on the field mirror after a series of changes is 15 mm, so the focused spot diameter D can be calculated by the above equation to be about 8.24 μm.

Most methods to indirectly measure the spot through the line width of workpiece etching will be affected by various parameters and will have some errors. Using the process parameters and scanning strategy studied in the previous paper can produce a better microlens with a surface roughness of 1.6 μm in the setup area and achieve a flatter etched surface edge, which proves the feasibility of the processing scheme and process parameters.

4.2.2. Machining Error Compensation

The dynamic focusing system enables focal position adjustment during three-dimensional layered machining. However, the machining profile accuracy may also be affected by various factors, resulting in deviations between the actual machined profile and the theoretical model. After laser processing, a tactile profilometer was used to measure the profile accuracy of the microlens. The transverse residual error is calculated by subtracting the filtered data from the fitted spherical contour, and the transverse residual error is used to compensate for the transverse shape error.

The deviation between the actual machined profile and the theoretical model may be associated with factors such as plasma shielding, laser energy attenuation, and redeposited material. However, the contributions of these factors were not quantitatively evaluated in this study. To address the observed machining profile deviations, a conventional inverse model error compensation method was adopted based on the measured contours. Although the compensated machining results illustrate the application of this approach, the improvement in dimensional accuracy cannot be quantitatively assessed due to the lack of comparative form error data before and after compensation.

Using the compensated contour graphics to establish a three-dimensional model to compensate for the contour error, and, finally, processing the physical figure shown in Figure 12, the measured profile showed general agreement with the theoretical profile, and its surface roughness was also basically consistent, measured as 1.6 μm.

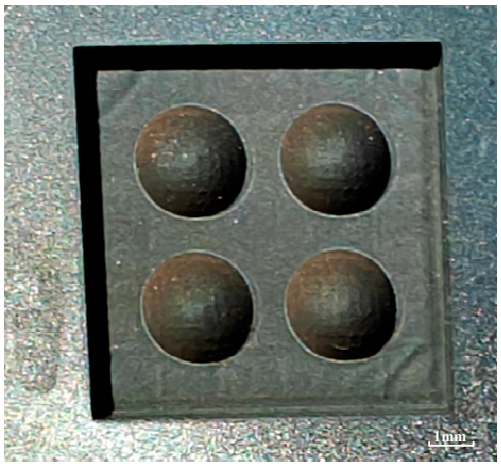


Figure 12. The 2 × 2 monocrystalline silicon lens array processing effect.

The proposed combined machining process demonstrates the feasibility of fabricating monocrystalline silicon microlens arrays on a small scale. In principle, the layered scanning strategy and model compensation method can be extended to arrays containing more microlens units. However, as the present experiments were limited to 2 × 2 and 4 × 4 arrays, the uniformity of surface morphology and dimensional accuracy over larger processing areas has not been systematically evaluated. For large-area arrays, factors such as variations in focusing conditions, positioning errors, and polishing uniformity may influence the consistency of individual microlenses. Therefore, further experimental investigation is required to evaluate the applicability and processing consistency of the proposed method for large-area microlens arrays.

4.3. Mirror Sandblasting and Polishing

The SMKS mirror sandblasting machine equipment was used for the finishing part of this experiment. The apparatus is capable of transporting abrasive grains of different types and particle sizes to the spray system, which are sprayed onto the surface of the workpieces to be processed under preset pressures and angles to realize precision grinding and polishing.

Considering the material properties of monocrystalline silicon, a rubber ball was selected as the abrasive particle carrier, and the outer surface was coated with a layer of nanometer-sized brick powder. The particle diameter of the abrasive is selected at 0–0.5 μm, the abrasive diameter at 300–400 μm, and the processing pressure is selected at 6 MPa. In order to ensure the consistency of processing, the processing degree of each angle needs to be consistent in the processing process, and the polishing angle is 360°. In the processing process, the workpiece needs to rotate at a uniform speed, and the polishing time is selected as 20 min to ensure mirror polishing and processing efficiency of the material.

In the finishing step, by machining a lens unit for the verification of finishing experiments, the surface morphology after polishing is shown in Figure 13, where it can be seen that the sandblasted and polished surface has obviously become much smoother, into a mirrored microlens array.

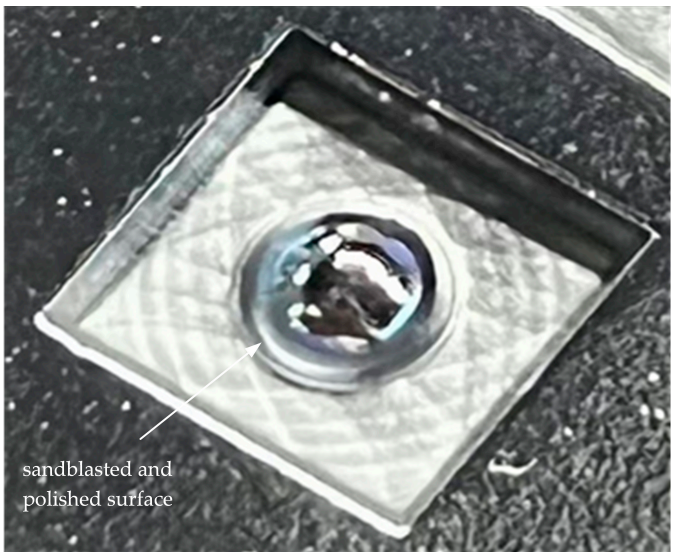


Figure 13. Physical drawing of sandblasted and polished finishing.

The measured profile shown in Figure 14 exhibits a relatively smooth curved shape, with a surface roughness Ra of approximately 100 nm after polishing, indicating an improvement in surface smoothness. Although the femtosecond laser can realize the initial processing of dimensional control, its relatively rough surface still needs further processing. Therefore, sandblasting–polishing is not only a complement to the preliminary processing, but also an indispensable and critical step to enhance the surface quality to mirror level.

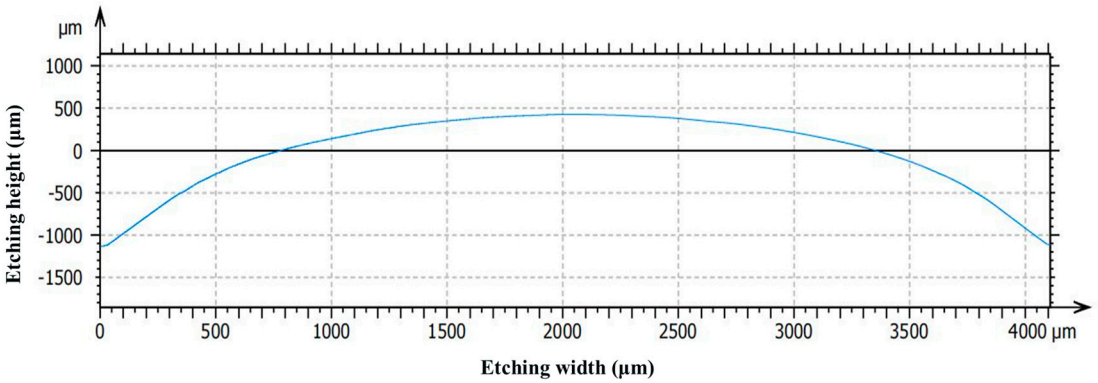


Figure 14. Contour measurement drawing.

During mirror sandblasting and polishing, abrasive particles interact with the workpiece surface under the applied pressure, contributing to the removal of surface irregularities. The observed reduction in surface roughness demonstrates the effectiveness of the finishing process, although the microscopic material removal mechanism has not been quantitatively verified. Furthermore, direct comparative experiments with conventional methods, such as ultra-precision turning and photolithography, were not conducted. Therefore, the present results do not establish the quantitative superiority of the proposed process in terms of machining accuracy, efficiency, or cost. In addition, the current surface characterization is mainly based on two-dimensional profile measurements, which cannot fully reveal the three-dimensional surface morphology or microscopic defect characteristics. Further quantitative analysis and characterization are required to provide a more comprehensive evaluation of the polishing process.

5. Conclusions

Monocrystalline silicon material is a hotspot for research and application, especially the outstanding performance characteristics have attracted much attention, and at the same time, its hardness, brittleness and high structural stability, which poses a considerable challenge to the traditional processing technology. In order to solve the problem of its processing difficulties, this paper proposes a femtosecond laser roughing–sandblasting polishing finishing single-crystal silicon microlens array processing process flow to explore new processing methods for hard and brittle materials processing microlens arrays and ultimately obtain a more perfect microlens array.

In this paper, the dynamic focusing system and F-Theta field mirror are designed and simulated based on the optical simulation software ZEMAX. The complete optical path diagram of the whole system is successfully simulated, and the floating of the laser focus after dynamic focusing and the F-Theta mirror is observed.

The influence mechanism of femtosecond laser power and galvanometer scanning speed on etching depth and surface roughness was investigated. The experimental results show that with the increase in femtosecond laser power, the etching depth and surface roughness increase to varying degrees; the increase in scanning speed leads to a rapid decrease in surface roughness and then an increase, and the etching depth decreases gradually. The effect of pulse accumulation on edge-quality machining was analyzed, and the on−off delay, idle delay and corner delay of the galvanometer were controlled by the time-delay method to optimize the edge quality of femtosecond laser machining.

The processing flow of laser machining of a microlens array was optimized by error compensation. After preliminary parameter research, the microlens array was processed by layered scanning; the processing morphology was improved by model compensation, and the surface was smoothed by sandblasting. Through experiments and simulations, 515 nm green light with a repetition frequency of 100 kHz was finally selected. The power is about 20 W; the scanning speed remains unchanged at 3000 mm/s and the scanning interval is 5 μm in the same direction; the light delay is 0.23 ms, the light delay is 0.12 ms, the angle delay is 0.13 ms and the idle delay is 0.24 ms; the layer height is 1 μm for laser processing; and the SMKS mirror sandblasting machine equipment is finished. The final surface roughness Ra decreases from 1.6 μm to 100 nm. The process parameters are feasible and the processing effect is good. It provides a new method for processing hard and brittle materials.

Author Contributions: Conceptualization, P.L. and Y.Z.; methodology, P.L., J.Y. and T.Z.; software, P.L. and A.X.; validation, P.L., J.Y. and W.Y.; formal analysis, P.L. and T.Z.; investigation, P.L., A.X. and W.Y.; resources, Y.Z.; data curation, P.L. and J.Y.; writing—original draft preparation, P.L.; writing—review and editing, P.L., J.Y., T.Z. and Y.Z.; visualization, P.L. and A.X.; supervision, T.Z. and Y.Z.; project administration, Y.Z.; funding acquisition, Y.Z. All authors have read and agreed to the published version of the manuscript.

Funding: This paper received funding from the National Natural Science Foundation of China (52375403, 52435008); Beijing Natural Science Foundation (L2611037); Open Fund of the National Key Laboratory of Advanced Off-Road System Technology (AF20240031); Beijing Institute of Technology Young Faculty Academic Launch Program (XSQD-202203014); Jiangsu Shuguang Optoelectronics Co., Ltd. (KY2024-06-006); and The New Generation Multi-Purpose Laser Irradiation System of Huiyan Action Project (654E88B6).

Institutional Review Board Statement: Not applicable.

Informed Consent Statement: Not applicable.

Data Availability Statement: Data underlying the results presented in this paper are not publicly available at this time but may be obtained from the authors upon reasonable request.

Acknowledgments: The authors gratefully acknowledge the valuable assistance provided by Hui Wu with the experimental investigations and measurements reported in this work.

Conflicts of Interest: The authors declare no conflicts of interest.

References

1. Pan, S.; Yang, Z.; Pan, Q.; Shen, W. Design of optical system for short-wave infrared silicon immersion grating imaging spectrometer; In *Seventh Symposium on Novel Photoelectronic Detection Technology and Applications*; SPIE: San Diego, CA, USA, 2020.
2. Liu, Y.; Zhu, J.; Chen, C.; Hou, X. Design of large-angle distortion-free and spot adjustable LED spot array projector based on microlens array and eyepiece. *Displays* **2023**, *79*, 102487.
3. Marin-Montin, J.; Ortiz-Roldan, J.M.; Hamad, S.; Montero-Chacón, F. Multiscale thermomechanical assessment of silicon carbide-based nanocomposites in solar energy harvesting applications. *Appl. Therm. Eng.* **2023**, *235*, 121400.
4. Tilli, M.; Paulasto-Kröckel, M.; Motooka, T.; Lindroos, V.; Airaksinen, V.M.; Franssila, S.; Lehto, A. *Handbook of Silicon Based MEMS Materials and Technologies*, 2nd ed.; Elsevier: Miamisburg, OH, USA, 2015.
5. Zhou, T.; Xie, J.; Liang, Z.; Liu, X.; Liu, X.; Wang, X. Research progress and prospects of optical microlens array compression molding. *Chin. Opt.* **2017**, *10*, 603–618. (In Chinese)
6. Chen, C.F.; Tzeng, S.D.; Chen, H.Y. Silicon microlens structures fabricated by scanning-probe gray-scale oxidation. *Opt. Lett.* **2005**, *30*, 652–654.
7. Cui, D.; Li, S. Review on ductile regime machining of hard and brittle materials. *Ordnance Mater. Sci. Eng.* **2014**, *37*, 125–132.
8. Mukaida, M.; Yan, J. Ductile machining of single-crystal silicon for microlens arrays by ultraprecision diamond turning using a slow tool servo. *Int. J. Mach. Tools Manuf.* **2017**, *115*, 2–14.
9. Sun, Q.; Tang, J.; Shen, L.; Lan, J.; Shen, Z.; Xiao, J.; Chen, X.; Zhang, J.; Wu, Y.; Xu, J.; et al. Fabrication of High Precision Silicon Spherical Microlens Arrays by Hot Embossing Process. *Micromachines* **2022**, *13*, 899.
10. Hua, J.G.; Ren, H.; Jia, A.; Tian, Z.N.; Wang, L.; Juodkazis, S.; Chen, Q.-D.; Sun, H.-B. Convex silica microlens arrays via femtosecond laser writing. *Opt. Lett.* **2020**, *45*, 636–639.
11. Albero, J.; Nieradko, L.; Gorecki, C.; Ottevaere, H.; Gomez, V.; Thienpont, H.; Pietarinen, J.; Päivänranta, B.; Passilly, N. Fabrication of spherical microlenses by a combination of isotropic wet etching of silicon and molding techniques. *Opt. Express* **2009**, *17*, 6283–6292.
12. Liu, X.Q.; Chen, Q.D.; Guan, K.M.; Ma, Z.; Yu, Y.; Li, Q.; Tian, Z.; Sun, H. Dry-etching assisted femtosecond laser machining. *Laser Photonics Rev.* **2017**, *11*, 1600115.
13. Sugioka, K.; Cheng, Y. Femtosecond laser processing for optofluidic fabrication. *Lab A Chip* **2012**, *12*, 3576.
14. Wang, B.X.; Zheng, J.X.; Qi, J.Y.; Guo, M.R.; Gao, B.R.; Liu, X.Q. Integration of Multifocal Microlens Array on Silicon Microcantilever via Femtosecond-Laser-Assisted Etching Technology. *Micromachines* **2022**, *13*, 218.
15. Yang, C.C.; Yang, C.C.; Hsu, C.N.; Huang, K.C.; Tseng, S.F.; Hsiao, W.T. Multilayer stack materials on silicon-based wafer dicing processes using ultraviolet laser direct dicing and milling methods. *Opt. Laser Technol.* **2018**, *108*, 441–449.
16. Jiang, T.; Zhao, Q.L.; Dong, Z.W.; Fan, R.W.; Yu, X. Interaction mechanism of femtosecond laser and wide band-gap material. *Infrared Laser Eng.* **2010**, *39*, 1044–1048.
17. Chen, S.L.; ONeil, W. The effects of power rippling on CO_2 laser cutting. *Opt. Laser Technol.* **1997**, *29*, 125–134.
18. Grigoropoulos, C.P. *Transport in Laser Microfabrication: Fundamentals of Laser Energy Absorption*; Cambridge University Press: Cambridge, UK, 2009.
19. Hardik, V.; Stephan, K.; Paul-Tiberiu, M. Thermal and non-thermal ablation mechanisms in crystalline silicon by femtosecond laser pulses: Classical approach of the carrier density two temperature model. *J. Phys. D. Appl. Phys.* **2022**, *55*, 175109.
20. Liu, Y.H.; Kuo, K.; Cheng, C.; Lee, A.-C. Femtosecond laser two-beam interference applied to 4H-SiC surface hierarchical micro-nano structure fabrication. *Opt. Laser Technol.* **2022**, *151*, 108081.
21. Appleyard, D.C.; Lang, M.J. Active particle control through silicon using conventional optical trapping techniques. *R. Soc. Chem.* **2007**, *7*, 1837–1840.
22. Feng, T.; Chen, G.; Han, H.; Qiao, J. Femtosecond-Laser-Ablation Dynamics in Silicon Revealed by Transient Reflectivity Change. *Micromachines* **2021**, *13*, 14.

23. Zhang, H.; Hasegawa, S.; Toyoda, H.; Hayasaki, Y. Three-dimensional holographic parallel focusing with feedback control for femtosecond laser processing. *Opt. Lasers Eng.* **2022**, *151*, 106884.
24. Jiří, N.; Antonín, M. Method for algebraic calculation of initial design parameters of a two-element telecentric f-theta lens. *Appl. Opt.* **2023**, *62*, 6113–6119.

Disclaimer/Publisher's Note: The statements, opinions and data contained in all publications are solely those of the individual author(s) and contributor(s) and not of MDPI and/or the editor(s). MDPI and/or the editor(s) disclaim responsibility for any injury to people or property resulting from any ideas, methods, instructions or products referred to in the content.